JCI insight

Potential limitations of micro-dystrophin gene therapy for Duchenne muscular dystrophy

Cora C. Hart, … , David W. Hammers, H. Lee Sweeney

JCI Insight. 2024. https://doi.org/10.1172/jci.insight.165869.

Research In-Press Preview Muscle biology Therapeutics

Clinical trials delivering high doses of adeno-associated viruses (AAVs) expressing truncated dystrophin molecules (micro-dystrophins) are underway for individuals with Duchenne muscular dystrophy (DMD). We examined the efficiency and efficacy of this strategy with four micro-dystrophin constructs (three in clinical trials and a variant of the largest clinical construct), in a severe mouse model of DMD, using doses of AAV comparable to those used in the clinical trials. We achieved high levels of micro-dystrophin expression in striated muscle with cardiac expression ~10 fold higher than that observed in skeletal muscle. Significant, albeit incomplete, correction of the skeletal muscle disease was observed. Surprisingly, a lethal acceleration of cardiac disease progression occurred with two of the micro-dystrophins. The detrimental impact on the heart appears to be caused by the high levels of micro-dystrophin resulting in variable competition (dependent on the design of the micro-dystrophin) between micro-dystrophin and utrophin at the cardiomyocyte membrane. There may also be a contribution from an overloading of protein degradation. The significance of these observations for patients currently being treated with AAV-micro-dystrophin therapies is unclear since the levels of expression being achieved in the DMD hearts are unknown. However, it suggests that micro-dystrophin treatments need to avoid excessively high levels of expression in the heart and cardiac function should be carefully monitored in these patients.

Potential limitations of micro-dystrophin gene therapy for Duchenne muscular dystrophy

Cora C. Hart[1,2,5], Young il Lee[1,2,5], Jun Xie[3], Guangping Gao[3], Brian L. Lin[4], David W. Hammers[1,2,6], H. Lee Sweeney[1,2,6]*

*[1]Department of Pharmacology & Therapeutics and [2]Myology Institute, University of Florida College of Medicine; Gainesville, FL 32610; [3]Horae Gene Therapy Center, University of Massachusetts Medical School, Worchester, MA 01655; [4]Department of Cell Biology, Neurobiology, and Anatomy & Department of Pediatrics, Medical College of Wisconsin; Milwaukee, WI 53226; [5]Equal contributions by these authors; [6]Equal contributions by these authors; *Corresponding author*

Correspondence: H. Lee Sweeney

1200 Newell Dr.

ARB R5-216

Gainesville, FL 32610-0267

Phone: 352-273-9416

Fax: 352-392-3558

Email: lsweeney@ufl.edu

ABSTRACT

Clinical trials delivering high doses of adeno-associated viruses (AAVs) expressing truncated dystrophin molecules (micro-dystrophins) are underway for Duchenne muscular dystrophy (DMD). We examined the efficiency and efficacy of this strategy with four micro-dystrophin constructs (three in clinical trials and a variant of the largest clinical construct), in a severe mouse model of DMD, using AAV doses comparable to those in clinical trials. We achieved high levels of micro-dystrophin expression in striated muscles with cardiac expression ~10 fold higher than that observed in skeletal muscle. Significant, albeit incomplete, correction of skeletal muscle disease was observed. Surprisingly, a lethal acceleration of cardiac disease occurred with two of the micro-dystrophins. The detrimental cardiac impact appears to be caused by variable competition (dependent on micro-dystrophin design and expression level) between micro-dystrophin and utrophin at the cardiomyocyte membrane. There may also be a contribution from an overloading of protein degradation. The significance of these observations for patients currently being treated with AAV-micro-dystrophin therapies is unclear since the levels of expression being achieved in the DMD hearts are unknown. However, it suggests that micro-dystrophin treatments need to avoid excessively high levels of expression in the heart and cardiac function should be carefully monitored in these patients.

INTRODUCTION

Duchenne muscular dystrophy (DMD) is an X-linked disorder that affects approximately 1 in 5000 newborn males (1). It is the most common of the childhood muscular dystrophies and results from the lack of the membrane-associated protein, dystrophin, which is critical for proper force transmission in muscle cells (2, 3). The loss of dystrophin results in hypersensitivity to injury in the skeletal muscle and leads to cardiac dysfunction. The skeletal muscle initially undergoes rounds of injury and repair, but repair eventually begins to fail, and the muscles are replaced with fibrosis and fat. The muscle loss progresses from proximal to distal, with the loss of respiratory muscles and/or heart failure as the cause of death, generally in the second or third decade of life (4). The cardiac disease manifests first with diastolic dysfunction and later progresses to a dilated cardiomyopathy (DCM) and failure (5-8).

Gene therapy for DMD has entered the clinic in the form of several versions of a highly truncated dystrophin (micro-dystrophin) delivered via adeno-associated virus (AAV). While AAV is highly efficient at infecting and transducing striated muscle, its small packaging capacity (~5 kb) makes it impossible to accommodate the full-length dystrophin coding sequence (~14 kb). This has necessitated using AAV to deliver the coding sequence of a highly truncated dystrophin (9, 10) or to use AAV to alter splicing of an out-of-frame dystrophin mRNA to create a deletion that restores the proper reading frame (11, 12). In either case, the goal is to express a truncated version of dystrophin to slow disease progression. This strategy essentially aims to transform DMD into a slower progressing muscular dystrophy, potentially more like some forms of Becker muscular dystrophy (BMD), a disease caused by dystrophin mutations that create in-frame transcripts resulting in production of a variety of truncated forms of dystrophin that are associated with different rates of disease progression.

A number of questions surround the outcome of these trials, particularly the dosing and the potential efficacy of each of the different micro-dystrophin constructs currently in trial. It is unclear when and if there will be a need to redeliver the therapy due either to dilution of transduced

nuclei from muscle growth, or to skeletal muscle turnover due to residual muscle degeneration or general myonuclear loss, resulting in eventual loss of the AAV DNA encoding the micro-dystrophin transgene. Thus, a major clinical goal is to express the micro-dystrophin at high levels throughout the skeletal and cardiac muscles, which potentially will limit the frequency of needing to redeliver AAV to the skeletal muscle. Since the cardiomyocytes do not turnover, redelivery will be unnecessary unless they were not adequately transduced with the first dose of virus.

Most of the preclinical work supporting these DMD trials was performed using dystrophic mice of C57-based genetic backgrounds, which exhibit mild disease progression when compared to that of other mouse genetic backgrounds (13) and larger mammals (14, 15). While information concerning transgene delivery and expression can be gathered using these C57-based models, it is difficult to assess the translational efficacy of AAV-micro-dystrophin gene therapies at correcting a severe, life-limiting striated muscle disease. Indeed, the lack of an animal model that is completely representative of the human disease has contributed to the discrepancy in results between preclinical and clinical research and has ultimately resulted in the termination of several DMD clinical trials (16). Therefore, this study utilized a severe mouse model of DMD, the D2.*mdx* mouse harboring the *mdx* mutation on the DBA/2J genetic background (13, 17, 18) to evaluate the long-term impact of AAV driven micro-dystrophin on the heart and skeletal muscles in the face of a more aggressive disease progression.

Common features of micro-dystrophin constructs (shown in **Figure 1**) include the N-terminal actin-binding region, four to five of the twenty-four spectrin-like triple helical bundles that make up the rod region, and a truncated C-terminus containing the β-dystroglycan binding site. In this work, we sought to directly compare the efficiency and long-term efficacy of three clinical versions, which we refer to as MDC1, MDC2, and MDC3 (see **Figure 1**). Given the size of the promoter (CK8) we used for these comparisons, the size of MDC3 exceeded the efficient packaging limit of AAV. Thus, we also included a smaller, published variant of MDC3 that differs only by the deletion of hinge (H) 3 [MDC4; aka Δ3849 (9)]. This smaller variant showed no

significant difference in efficacy compared to MDC3 in the initial report (9) and demonstrated skeletal muscle rescue in a C57-based transgenic model (19).

In this head-to-head evaluation, we sought to determine the long-term efficacy of these four micro-dystrophins at correcting the skeletal and cardiac muscle pathologies associated with the D2.*mdx* mouse model of DMD. As depicted in **Figure 2A**, this experiment consisted of male D2.*mdx* mice receiving an intravenously (IV) delivered dose of AAV-packaged, codon-optimized human micro-dystrophin at 1 month of age. All constructs were placed behind the CK8 striated muscle promoter (20) and packaged in AAVrh10 serotype vector, which has a high tropism for striated muscle (21) and shares 98.8% of its identity with AAVrh74, a vector utilized in one micro-dystrophin clinical trial (22).

Using a clinical AAV dose [$2x10^{14}$ gc/kg (23)], we observed widespread transduction and sustained expression of all four micro-dystrophins in skeletal and cardiac muscles of D2.*mdx* mice with the heart achieving much greater overexpression – compared to endogenous dystrophin – that is ~5-10 fold higher than in skeletal muscles. All treatments slowed skeletal muscle disease progression to some degree, although not completely stopping it. Surprisingly, the overexpression of two of the micro-dystrophins (MDC1 and MDC4; see **Figure 1**) led to an accelerated onset of a DCM, heart failure and death. These mouse studies highlight the differential long-term efficacy achieved by different micro-dystrophin constructs but also caution against their overexpression in the heart. As we demonstrate, achieving high level expression of micro-dystrophin in the heart may be deleterious, depending on the construct design.

RESULTS

Clinical AAV doses enable widespread expression in D2.mdx striated muscle.

As depicted in the experimental schematic in **Figure 2A**, AAV was administered systemically through the tail vein at a dose of $2x10^{14}$ gc/kg, which is currently used in the clinic (23). The treatment of D2.*mdx* mice in this manner resulted in equivalent striated muscle expression of the three largest micro-dystrophins, MDC2, MDC3 and MDC4 (**Figure 2C**). The smallest construct, MDC1, achieved much higher levels of expression in striated muscle (**Figure 2C;** ~7-fold greater). We observed robust and uniform expression of all micro-dystrophins at the sarcolemma of cardiomyocytes, as detected by immunofluorescence (**Figure 2E,** top panel). The expression of micro-dystrophin coincided with an increase in membrane-associated content of the dystrophin-glycoprotein complex (DGC) members β-dystroglycan, syntrophin and dystrobrevin (**Figure 2E**).

Immunoblotting data estimate that the micro-dystrophin levels achieved by this treatment for the three largest micro-dystrophins greatly exceed wild-type levels of native dystrophin in both the gastrocnemius and heart (**Figure 2D**; ~5- and ~55-fold greater, respectively). The relatively high expression level of MDC1 in comparison of the other micro-dystrophins is not due to high viral transduction, as vector genome content in the heart is not proportional to protein levels (**Supplemental Figure 1**). These results demonstrate that the treatment of D2.*mdx* mice with clinical doses of AAV-packaged micro-dystrophin leads to efficient transduction and micro-dystrophin expression in both skeletal and cardiac muscle. Despite equivalent micro-dystrophin levels being achieved by the three largest constructs, we observed a striking difference in survival age between the treatment groups; MDCs 1 and 4 lead to a premature death (**Figure 2B**). Therefore, the terminal measures for surviving mice receiving MDC1 and MDC4 were conducted at 12 months, while those for MDC2 and MDC3 treatments occurred at 18 months of age, with appropriate age-matched controls for each endpoint (**Figure 2A**).

Micro-dystrophin gene therapy partially corrects the D2.mdx skeletal muscle pathology.

At terminal endpoint*, ex vivo* functional evaluations of diaphragm and extensor digitorum longus (EDL) muscles were performed. As anticipated by previous reports (10, 24, 25), micro-dystrophin treatment improved several features of skeletal muscle function including increases in diaphragm specific tension, EDL specific tension, and EDL resistance to eccentric contraction-induced functional deficits, compared to untreated D2.*mdx* mice (**Figure 3A-D**). However, these functional improvements were, for the most part, significantly diminished compared to D2.WT values. One of the clinical constructs, MDC3, provided much less benefit to the skeletal muscle than the other three constructs (**Figure 3A-D**). In agreement with a partial skeletal muscle rescue by micro-dystrophin, the diaphragms of treated mice exhibited fibrotic lesions, albeit less than untreated D2.*mdx* animals (**Figure 3E**). Additionally, all MDCs significantly reduced fibrosis in the gastrocnemius (**Figure 3E**). Systemic micro-dystrophin gene therapy provides significant, albeit incomplete, rescue of D2.*mdx* skeletal muscle. The resulting phenotype appears to lie within the spectrum of a BMD-like disease, which likely represents an approximate ceiling of what would be expected of micro-dystrophin's efficacy in the clinic.

Micro-dystrophin gene therapy may not benefit D2.mdx hearts.

During the course of this study, longitudinal changes in cardiac function were assessed by collecting electrocardiograms and echocardiograms of all treatment groups at 6 and 12 months of age, and additional 18-month measurements for mice that received MDCs 2 or 3. At 6 months of age, untreated D2.*mdx* hearts do not exhibit significant differences in function from D2.WT hearts; however, mice treated with MDCs 3 or 4 have increased left ventricular chambers (**Figure 4A**; end diastolic volume) and this was accompanied by a decrease in ejection fraction in mice treated with MDC3 (**Figure 4B**). Mice that received MDC1 have a reduced stroke volume (SV) and subsequent reduction in cardiac output (CO) at 6 months of age (**Supplemental Table 1**).

By 12 months of age, D2.*mdx* mice exhibit cardiac dysfunction: left ventricular restriction as evidenced by a decrease in end diastolic volume (EDV; **Figure 4A**) that results in a decrease in SV and CO (**Supplemental Table 2**). Other parameters of diastolic dysfunction exhibited by D2.*mdx* mice include an elevated isovolumic relaxation time (IVRT), a decreased mitral valve early (MV E) velocity, and an impaired myocardial performance index (MPI; **Supplemental Table 2**). Likewise, mice treated with MDC2 display left ventricular restriction (a decrease in EDV; **Figure 4A**) that results in a decrease in SV and CO (**Supplemental Table 2**). In contrast, animals treated with either MDC 1 or 4 dilate at 12 months of age (increase in EDV; **Figure 4A**) and have a significant decrease in ejection fraction (EF; **Figure 4B**). Additionally, a subset of MDC1-treated animals exhibits no discernable MV A wave, visualized with pulsed-wave Doppler, have a compensatory increase in MV E, and therefore have an elevated E/A ratio (**Supplemental Table 2**). In agreement with their profound effect on survival (**Figure 2B**), MDC1 and MDC4 induce a severe cardiomyopathy with features of a dilated cardiomyopathy (DCM).

By 18 months of age, MDC2 treated animals developed a DCM characterized by dilation (**Figure 4A**) and decreased systolic function (**Figure 4B**). In contrast, 18-month-old MDC3 treated animals have a sustained ejection fraction (**Figure 4B**) and a normalized end diastolic volume (**Figure 4A**). Unlike the findings in the gastrocnemius and diaphragm (**Figure 3E)**, cardiac fibrosis was differentially impacted by MDC treatments. MDC3 treated animals did not develop a DCM and had reduced cardiac fibrosis (**Figure 4C**). While MDC3 had the least impact on skeletal muscle, it best protected the heart in this study. Moreover, none of the MDCs were able to correct all of the electrocardiogram abnormalities observed in D2.*mdx* mice (**Supplemental Figure 2** and **Supplemental Tables 4-6**).

When assessing two of the MDCs with differential impacts on the heart at 12 months of age, MDC 2 and 4, we found that each construct had a different impact on cardiomyocyte calcium transients. Consistent with known Ca^{2+} overload signaling in DMD, D2.*mdx* cardiomyocytes exhibit elevated Ca^{2+} levels, and MDC2 normalized peak Ca^{2+} release and % sarcomere length

shortening (**Supplemental Figure 5**). In contrast, MDC4 exacerbates peak Ca^{2+} release without any normalization in contractility, potentially contributing to heart failure and premature death observed in MDC4-treated D2.*mdx* mice. Collectively, these data indicate that AAV-micro-dystrophin treatment can potentially have a detrimental impact on the heart, depending on the micro-dystrophin design and expression levels.

Potential mechanisms contributing to micro-dystrophin-induced cardiomyopathy.

We sought to explore potential mechanisms contributing to these detrimental cardiac outcomes. These investigations have led us to suspect two potential causes of this micro-dystrophin-induced cardiomyopathy: **a)** micro-dystrophin competes with and displaces endogenously-expressed utrophin at the cardiomyocyte sarcolemma and **b)** the long-term overexpression of micro-dystrophin protein contributes to overload of the ubiquitin-proteosomal system (UPS), resulting in impairments in cardiomyocyte protein quality control. We present below the data and observations in support of the first mechanism (utrophin displacement) as the main contributor to micro-dystrophin-induced acceleration of cardiomyopathy, and overload of the ubiquitin-proteosomal system (UPS) occurring if the expression levels are high enough (as with MDC1).

The heart normally expresses a combination of utrophin and dystrophin, with potential overlapping and distinct roles that have yet to be elucidated. The ability of these two orthologous proteins to link the cytoskeleton to the extracellular matrix through their interactions with common partners is consistent with some degree of functional redundancy. Indeed, utrophin protein levels in the heart increase in absence of dystrophin (26-28), and the removal of utrophin worsens the cardiac phenotype in the B10.*mdx* mice (29-31), with the total removal of utrophin being worse than haploinsufficiency. Thus, it is clear that utrophin can partially mitigate the loss of dystrophin. To potentially explain how high levels of micro-dystrophin leads to cardiomyopathy, we sought to determine if micro-dystrophin displaces utrophin from the cardiomyocyte membrane, as it is

possible that strong overexpression of micro-dystrophin may phenocopy utrophin ablation via replacement with a truncated, and potentially less functional, dystrophin molecule. Therefore, we assessed the relative amounts of utrophin at the cardiac membrane by immunoblotting of membrane enriched fractions of cardiac extracts from D2.WT, untreated D2.*mdx,* and micro-dystrophin-treated D2.*mdx* mice, in order to discern whether micro-dystrophin reduces membrane-associated utrophin in D2.*mdx*. The hearts of D2.*mdx* mice treated with either the MDC1 or the MDC4 micro-dystrophin exhibited significant decreases in utrophin immunoreactivity at the membrane to ~60% of D2.WT levels and ~30% of D2.*mdx* levels (**Figure 5A-B**). In contrast, neither the MDC2 nor MDC3 micro-dystrophin displaced utrophin to the same extent.

This potential for micro-dystrophins to outcompete utrophin for association with the sarcolemma is not restricted to cardiomyocytes: AAV-mediated MDC4 expression in D2.*mdx* skeletal muscle also results in utrophin displacement from muscle fiber sarcolemma (**Supplemental Figure 4A**). Micro-dystrophin and utrophin thus appear to display a complementary and mutually exclusive pattern of expression in both heart and skeletal muscles of micro-dystrophin-treated D2.*mdx* mice. This likely results from competition between the two proteins for common binding partners present within the sarcolemma. There are two sites in wild-type skeletal muscle fibers where utrophin, along with dystrophin, accumulates at high density: the neuromuscular junction (NMJ) and the myotendinous junction (MTJ). Utrophin accumulation at these specialized portions of myofibers appear unperturbed despite overexpression of micro-dystrophin (**Supplemental Figure 4B-C**). The absence of any noticeable utrophin depletion by micro-dystrophins at NMJs could result from the assembly of specialized sub-regions of the post-synaptic apparatus in which dystrophin (along with voltage-gated sodium channels) and utrophin (together with nicotinic acetylcholine receptors; nAChRs) are spatially segregated (32-37). Such organization suggests distinct interactions that recruit dystrophin and utrophin to their respective domains with specificity. The degree of micro-dystrophin overexpression in skeletal muscle achieved in these experiments (approximately 10-fold lower than in the heart) may be insufficient

to overcome utrophin's affinity to its interacting proteins at the NMJs. Alternatively, but not mutually exclusive, the sheer density of utrophin at NMJs and MTJs that appears to far exceed the extrajunctional sarcolemma (**Supplemental Figure 4B-C**) making competition from micro-dystrophin less effective at these specialized membrane structures. In the case of NMJs, the density of nAChRs at the NMJs is measured to be up to 1000-fold greater than at the extrasynaptic portions of the myofiber surface (38). While it is unknown whether utrophin levels at NMJs reach that of the nAChRs, its concentration at the synapse, as well as its potential to form protein interactions distinct from those of dystrophin, likely help maintain high-density synaptic accumulation of utrophin despite micro-dystrophin overexpression.

Another potential mechanism by which micro-dystrophin expression leads to cardiomyopathy, potentially in combination with utrophin displacement, is the saturation of the UPS by the excess micro-dystrophin molecules. Postmitotic cells, including cardiomyocytes, are especially susceptible to proteotoxicity stemming from accumulation of misfolded proteins, and impaired cardiomyocyte protein homeostasis has been shown to cause DCM-like cardiac phenotypes (39, 40). The sheer degree of overexpression (~50 fold higher than endogenous dystrophin of wild-type hearts) may saturate the capacity of the cardiomyocytes to ensure that proteins maintain their functional conformation and to breakdown/recycle those that are misfolded or damaged. Accumulation of polyubiquitinated proteins can serve as a molecular signature for UPS saturation and can lead to cardiomyopathy by impairing both the proper clearing of damaged/misfolded proteins and the timely turnover of typically short-lived proteins with specific signaling or transcriptional roles (41, 42). The AAV-mediated treatment of D2.*mdx* mice with the 4-repeat micro-dystrophin (MDC1) whose overexpression far exceeds the levels achieved by the 5-repeat variants (**Figure 2C**) produced a significant increase (~3-fold vs untreated D2.*mdx*) in the accumulation of K48 linkage-specific polyubiquitinated protein in the hearts (**Supplemental Figure 3**). Although, these findings do not conclusively establish disrupted protein homeostasis in cardiomyocytes as a major cause of DCM in D2.*mdx* hearts, the data presented are consistent

with the hypothesis that impaired protein quality check in cardiomyocytes may accelerate the progression toward heart failure coupled with another contributing disease mechanism.

DISCUSSION

Micro-dystrophin gene therapy clinical trials are currently underway for the treatment of DMD. In the current report, we sought to critically examine the long-term efficacy of four different micro-dystrophin gene therapies using a severe mouse model of DMD to better understand the impact and potential limitations of these emerging therapeutics for the treatment of DMD. Previously, we demonstrated that the DBA/2J background strain does not exhibit an inherent cardiomyopathy (43), validating it as a useful background strain for this study. While there are numerous pre-clinical publications evaluating the efficacy of systemic AAV-mediated delivery of micro-dystrophin, many of these studies did not assess cardiac function (25, 44-46). Of the studies that did evaluate cardiac function (via EKG and pressure-volume catheters), a lower AAV dose than was used in the current study (and current clinical trials) was used, and/or the short study length would have prevented observing a progression to heart failure (24, 47-50). Therefore, to our knowledge, this is the first study that has assessed the long-term cardiac function of a severe mouse model of DMD following micro-dystrophin gene therapy using the high dose of AAV being used in clinical trials, albeit with a promoter that likely is stronger in the heart than those used in two of the clinical trials (51). A summary of our findings can be found in **Table 1**.

The dose of AAV (2×10^{14} gc/kg) used for this study was chosen to mirror doses being used in ongoing clinical trials with AAV-micro-dystrophin in DMD patients (23). Clinical implementation of this dose has been dictated by the attempt to transduce as many skeletal muscle fibers as possible, which is assessed by post-injection muscle biopsies (23). There has been no consideration, however, of what this dose escalation may mean for the heart, and adequate modeling of these high doses and their long-term impact on the heart has not been previously performed. Furthermore, this work demonstrates that promoters that drive high level expression of the transgene in skeletal muscles are desirable, but lower-level expression in the heart is needed. Fortunately, it appears that the only trial using CK8, which is strong in skeletal muscle

and in the heart, is using a micro-dystrophin that is tolerated at higher expression levels in the heart, MDC2. The degree of cardiac expression achieved in preclinical models and DMD patients is dependent on the efficiency of cardiac muscle infection of the AAV capsid serotype used and the strength of the promoter in the heart. Based on the differential amounts of transgene expression we (**Figure 2C**) and others (46) have noted between murine skeletal and cardiac muscles, it is reasonable to assume that the heart is receiving more vector per cell than the skeletal muscle fibers (52). All of the promoters being used in the clinical trials were optimized for expression in both muscle types in mice, but the levels of expression in the human heart are unclear. The MHCK7 promotor driving MDC1 in clinical trials has been shown to have much greater expression in hearts than in skeletal muscle in mice (46, 53). Indeed, this promotor was said to be chosen for its high cardiac expression (23); however, the alpha myosin heavy chain enhancer (*Myh6*) that drives the high expression in mouse hearts will not achieve this in humans as alpha myosin heavy chain is not expressed in human ventricles (54). Alpha myosin heavy chain is highly expressed in human atria (54), however, and it is currently unknown how this expression pattern will impact conductivity or atrial function in humans. An update on one of the clinical trials reported promising gene therapy transduction and micro-dystrophin expression in the skeletal muscles of trial participants 1 year following treatment (23). This micro-dystrophin has since received conditional FDA approval. However, the level of cardiac micro-dystrophin expression that is being achieved in DMD patients remains unknown.

Micro-dystrophin partially rescues skeletal muscle disease in D2.mdx mice.

The potential to modify a severe DMD disease using a truncated dystrophin molecule was initially suggested by the existence of mildly-progressing BMD patients that express mutant dystrophin proteins missing most of the rod domain (55, 56). Therefore, the ultimate goal of micro-dystrophin gene therapy is to convert DMD into a milder disease. Herein, we identified that long-term treatment of D2.*mdx* mice with AAV-packaged micro-dystrophins that are similar to the three

clinical versions results in widespread transduction of the skeletal muscle and slowing of, but not halting, the progression of skeletal muscle disease. The treated muscles exhibit a slower progressing muscular degenerative disease, suggesting a conversion from DMD to a BMD-like pathology. Indeed, we find that the long-term trajectory of the skeletal muscle phenotype of micro-dystrophin-treated D2.*mdx* mice does represent a milder dystrophy, with progressive pathology most notable in the diaphragm. This progressive myopathy does not appear to be due to loss of micro-dystrophin in the mice over time (**Figure 2E**, bottom panel), as we initially anticipated, but rather is caused by the failure of micro-dystrophin to rescue all functions of full-length dystrophin, as in BMD.

It is likely that different designs of micro-dystrophin may slow the skeletal muscle disease to varying degrees, as we see a less robust rescue of the skeletal muscles with MDC3 as compared to MDC1, MDC2 and MDC4. The micro-dystrophin MDC2 construct is able to restore nNOS to the skeletal muscle membrane (24, 25), which may provide additional benefits to the skeletal muscle beyond sarcolemmal stability. Indeed, the diaphragm appears to be better rescued by this micro-dystrophin than by MDC3 (**Figure 3A**). This same region does not bind nNOS in the heart (57) but may serve other functions in the heart (58) and may have provided benefit that delayed the onset of DCM in the treated hearts, even though there was no impact on the onset of diastolic dysfunction (**Figure 4A**). On the other hand, MDC1 may exhibit increased membrane binding in the heart by the inclusion of repeats 1, 2, and 3, which may enhance membrane localization and functional stability of the micro-dystrophin protein (59). Attempts to restore some or all of the missing C-terminus in order to better reconstitute the membrane complex may also improve function and further slow disease progression. However, it is becoming increasingly clear that all regions of dystrophin serve specific roles, thus, any micro-dystrophin is likely to be a physiological compromise as compared to full-length dystrophin and, potentially, utrophin. Only animal models that recapitulate aspects of the human disease, such as the D2.*mdx* mouse, can reveal which compromises are likely the most efficacious for dystrophic

muscle. Ultimately it is likely that other types of therapies will need to be combined with micro-dystrophin gene therapy for the optimal management of DMD.

Micro-dystrophin overexpression can cause cardiomyopathy.

Surprisingly, the clinical dose of two of the AAV-micro-dystrophins tested resulted in the development of a severe and early onset life-limiting dilated cardiomyopathic failure. The very different cardiac outcome despite similar impact in the skeletal muscle does not appear to be due to the function of the micro-dystrophin *per se*. The premature onset of this cardiomyopathy appears to be related to the extent of micro-dystrophin overexpression in the heart and the specific design of the micro-dystrophin that alters its competition with utrophin for binding to the dystrophin-glycoprotein complex. For instance, despite similar expression levels between MCD2 and MCD4, the latter both hastens onset of cardiomyopathy and displaces utrophin to a larger extent. We provide evidence that micro-dystrophin expression at the levels achieved with the CK8 promoter via high dose AAV delivery causes displacement of native utrophin protein at the cardiomyocyte sarcolemma (dependent on micro-dystrophin design). The acceleration of the cardiomyopathy is co-incident with the efficient displacement of utrophin by two of the micro-dystrophins (MDC1 and MDC4). How well a specific micro-dystrophin functionally substitutes for utrophin or full-length dystrophin in the heart will depend on which regions are in the micro-dystrophin and which regions are most critical for proper cardiac function. Competition will likely depend not only on the degree of overexpression, but also on the design of the micro-dystrophin and its impact on binding partners, such as sytrophins, dystropbrevin, cavins, cryab, cypher, ahnak1 (57).

A recent study (60) demonstrated that micro-dystrophin is beneficial to the heart in the total absence of utrophin in a B10.*mdx* background. However, comparing that study with this study is difficult since the utrophin was missing from the heart throughout development, possibly allowing adaptations that cannot occur with acute postnatal displacement of utrophin by overexpression of

micro-dystrophin. In the absence of utrophin, we would predict that all micro-dystrophin constructs examined in this study should slow the onset of cardiac dysfunction and failure as compared to no intervention.

In contrast to our demonstration of micro-dystrophin outcompeting utrophin along the skeletal muscle fibers of the D2.*mdx* mice, but not at the neuromuscular and myotendinous junctions (**Supplemental Figure 4A**), the study from Krishna *et al*. was interpreted as demonstrating that micro-dystrophin does not compete with utrophin. This was based on their observation that AAV-delivered micro-dystrophin co-localizes with utrophin along the fibers in skeletal muscle (61). However, this was in a mouse that had higher levels of utrophin and lower levels of micro-dystrophin along the muscle fibers than in our case. They used dystrophin-deficient transgenic mice that expressed higher than normal levels of utrophin from all skeletal muscle nuclei and received about 10-fold less of an AAV-CK8-micro-dystrophin dose than in our mice, shifting the competitive advantage to utrophin.

The higher overexpression of a 4-repeat micro-dystrophin (MDC1) also produced evidence that suggests impaired protein quality check in cardiomyocytes. High level of transgene overexpression, in and of itself, can be detrimental if the increased protein turnover overloads the protein breakdown capacity of the cell (39) and likely puts an extra energetic load on an already stressed heart (62). Indeed, it was previously shown that 100-fold transgenic overexpression of a mini-dystrophin was associated with cardiac toxicity (63). This mini-dystrophin is likely more efficacious in the heart than any micro-dystrophin, which may allow higher levels of overexpression to be tolerated.

Our current data highlight the benefits, limitations, and potential deleterious consequences of maximizing micro-dystrophin overexpression in both skeletal and cardiac muscle for the treatment of DMD. Likely, all micro-dystrophin constructs would show some benefit in the heart if transgene expression levels are kept closer to physiological dystrophin levels to avoid pathological side effects that may include utrophin displacement or overload of the UPS.

Conclusion

Whether or not the DMD patients currently being dosed with AAV-micro-dystrophin in clinical trials are at risk of accelerated cardiac disease is unclear. It may be years before this question can be addressed, given that it requires 8-12 months to clearly see this cardiomyopathy development in mice. However, our preclinical data in mice suggest that there is reason to be concerned that while the skeletal muscles improve in individuals with DMD receiving the current AAV-micro-dystrophin vectors, the dystrophic hearts may not be improved by these treatments. Even if the treatment is modestly beneficial for the heart, the increased load on the heart due to the improved skeletal muscle function may accelerate the onset of DCM and heart failure. Therefore, frequent monitoring of the cardiac status of these patients should be performed and prophylactic use of cardio-protective drugs, including ACE inhibitors/angiotensin receptor blockers, beta-blockers, and/or mineralocorticoid receptor antagonists, should be considered. If the observations in this study are recapitulated in DMD patients, then micro-dystrophins may need to be optimized for cardiac rescue and delivery of micro-dystrophin to the heart may need to be dissociated from skeletal muscle via the use of promoters designed to drive less expression in the heart than in skeletal muscle.

METHODS & MATERIALS

Sex as a biological variable

This study only involved the use of male mice, as DMD is an X-linked disease that primarily affects human males.

Animals

This study used male D2.WT (Jax# 000671) and D2.*mdx* (Jax# 013141) mice from colonies originally obtained from Jackson Laboratory. Mice were housed 1-5 mice per cage, randomly assigned into groups, provided *ad libitum* access to food (NIH-31 Open formulation diet; Envigo #7917), water, and enrichment, and maintained on a 12-hour light/dark system.

Micro-dystrophin constructs and vector production

Codon-optimized μDys was synthesized by Genscript (Piscataway, NJ) and cloned into a pAAV shuttle plasmid containing the striated muscle-specific CK8 promoter (20) and a minimized synthetic polyadenylation signal sequence (64). AAV viral vector packaging was performed using the triple-transfection method, as previously described (21, 65).

Ex vivo muscle function

Maximal tetanic tension assessments of the EDL and diaphragm muscles were evaluated as previously described (66) by the University of Florida Physiological Assessment Core. Subsequently, a series of 5 eccentric contractions (stimulated at 80 Hz for 700 ms) with a stretch of 10% optimal length was imposed on the muscle in the last 200 ms of each contraction. Each contraction was separated by a 5-minute rest period. Following experimental procedures, muscles were weighed, frozen embedded in OCT or snap-frozen, and stored at -80 C until further use.

494 *Echocardiography and electrocardiograms*

495 Electrocardiograms and transthoracic echocardiograms were performed using the Vevo 3100
496 pre-clinical imaging system (Fujifilm Visualsonics). Mice were anesthetized using 3% isoflurane
497 and maintained at 1.5-2% to keep heart and respiration rates consistent among treatment groups.
498 Body temperature was maintained at 37℃ throughout imaging. Electrocardiograms were imported
499 into LabCharts (ADInstruments) for analysis. Four images were acquired for each animal: B-mode
500 parasternal long axis (LAX), B-mode short axis (SAX), M-mode SAX, and apical four-chamber
501 view with color doppler and pulsed-wave doppler. M-mode SAX images were acquired at the level
502 of the papillary muscle. Flow through the mitral valve was sampled at the point of highest velocity,
503 as indicated by aliasing, with the pulsed-wave angle matching the direction of flow. Images were
504 imported into Vevo LAB for analysis. Measurements of M-mode SAX and pulsed-wave doppler
505 images were made from three consecutive cardiac cycles between respirations.

506

507 *Fractionation, protein extraction, and immunoblotting*

508 Snap-frozen mouse heart and gastrocnemius muscles were finely crushed and homogenized in
509 a phosphate-based homogenization solution – 2 mM sodium phosphate, 80 mM NaCl, 1 mM
510 EDTA (67) – supplemented with 1 mM PMSF, phosphatase/protease inhibitor cocktail
511 (ThermoFisher Scientific), and centrifuged at 12,000 x g for 10 min at 4˚C. The supernatant
512 (soluble cytosolic fraction) is collected. The pelleted non-cytosolic (including membrane and
513 cytoskeletal) fraction is then re-suspended in the extraction buffer [homogenization solution
514 supplemented with the following: 20 µg/ml DNase I (Sigma), 10 µM Vinblastine (Caymen
515 Chemicals), 100 mM Swinholide A (Caymen Chemicals), 100 mM Mycalolide B (Focus
516 Biomolecules), 1% Digitonin (Biosynthe), 0.5% NP-40, 1% SDS] and extracted on-ice for 45-min
517 with occasional vortexing, followed by a 15-min incubation at 37˚C. The insoluble fraction was
518 pelleted by centrifugation at 12,000 x g for 10 min at 4˚C, and soluble membrane fraction was
519 collected. The protein concentration of soluble cytoplasmic and membrane fractions was

determined using the Bio-Rad Protein Assay (Bio-Rad Laboratories). Samples were boiled in 4X sample buffer, proteins separated using a 4-12% SDS polyacrylamide gels (ThermoFisher Scientific) and transferred to nitrocellulose membranes using the iBlot system (Life Technologies). Membranes were incubated at room temperature with 5% BSA-TBST, then overnight with primary antibodies at 4˚C. Following TBST washes and species-appropriate horseradish peroxidase-conjugated secondary antibody (Cell Signaling), incubated with ECL reagent (ThermoFisher Scientific), and imaged using the Li-Cor C-DiGit imaging system (Li-Cor Biosciences). Membranes were probed for GAPDH for cytosol/non-cytosol fractionation and stained with Ponceau S to control for equal protein loading and for normalization. The following primary antibodies were used for immunoblotting in the present study: MANHINGE1B (1:100; Clone 10F9; Developmental Studies Hybridoma Bank (DSHB)), MANEX1011B (1:100; Clone 1C7; DSHB), MANEX1011C (1:100; Clone 4F9; DSHB), utrophin-A (1:1000; ABN1739; EMD Millipore), Polyubiquitin (K48-linkage; 1:2000; #4389, Cell Signaling), and GAPDH (1:2000; SC-25778 ; Santa Cruz). Band signal intensities were measured using Image Studio Lite software (Li-Cor Biosciences), normalized to sample loading (Ponceau S stain), and reported relative to respective control samples.

Quantification of vector genomes

DNA was isolated from crushed heart samples using the DNeasy Blood & Tissue Kit (Qiagen #69506) following the manufacturer's instructions. Real-time PCR was performed with 100 ng of DNA from each sample using QuantiTect SYBR Green PCR Kit (Qiagen #204145). Primers used during this assay include those for codon optimized human micro-dystrophin (recognizes vector genomes; Forward: 5'- TGA CGC GTG GTA CCT CTA -3'; Reverse: 5'- GGA AGA TCC TAA TCG ATC ACA CA -3') and a genomic DNA region in the *Rpl32* locus of murine chromosome 6 (recognizes diploid genomes; Forward: 5'- GAG AAG GTT CAA GGG CCA GAT -3'; Reverse: 5'- AGC TCC TTG ACA TTG TGG ACC- 3'). Vector genome content was quantitated normalized to diploid vector genome expression using the ΔΔCT method.

Immunofluorescence and histological evaluations

Fresh-frozen OCT-embedded hearts and gastrocnemius muscles were sectioned at 10 µm and fixed in ice-cold acetone. The sections were re-hydrated in PBS, blocked in 5% BSA-PBS at room temperature and incubated with primary antibodies overnight at 4˚C. Mouse tissue sections to be incubated with mouse monoclonal antibodies were first incubated with a solution containing donkey anti-mouse IgG AffiniPure Fab fragments (1:25 in PBS; Jackson ImmunoResearch #715-007-003) for one hour prior to blocking. Following PBS washes, sections were incubated at room temperature with species- and isotype-appropriate fluorescent dye-conjugated secondary antibodies and coverslipped using Prolong Gold anti-fade mounting medium (ThermoFisher Scientific). The following primaries were used for immunofluorescence in the present study: MANHINGE1B (1:100; Clone 10F9; DSHB), MANEX1011B (1:100; Clone 1C7; DSHB), MANDAG2 (1:100; Clone 7A11; DSHB), utrophin-A (1:1000; ABN1739; EMD Millipore), utrophin (1:50; VP-U579; Vector Laboratories), Dystrobrevin (1:500; #610766; BD Biosciences); Syntrophins (1:2000; #11425; Abcam). NMJs were identified using fluorescent dye-conjugated α-bungarotoxin (1:500; ThermoFisher Scientific) to label nAchRs localized to the postsynaptic motor endplates. Image acquisition was performed with a Leica Application Suite X software on either a Leica TSC-8 confocal system or a Leica DMR epifluorescence microscope equipped with a Leica DCF480 digital camera. Comparative images were stained, imaged, and processed simultaneously under identical conditions.

Picrosirius Red (PSR) staining was performed as previously described (13) following decalcification of muscle sections using Formical-2000 (StatLab). Slides were visualized with a Leica DMR microscope, and images were acquired using a Leica DFC310FX camera interfaced with Leica LAS X software. Images were processed and analyzed by investigators blinded to study groups using ImageJ software.

Calcium kinetics

Harvested hearts were placed in a Langendorff setup, perfused with a Type II Collagenase (Worthington) and Protease (Sigma) digestion buffer and enzymatically digested. Cells were released by mechanical means, filtered via 200μm mesh filters, and spun down for further separation. The pellet of cells are plated and stepped up with Ca^{2+} to 1 mM over 30-45 minutes, and loaded with Fura-2AM Ca^{2+} dye. After reaching 1 mM Ca^{2+}, cells were assessed for simultaneous Ca^{2+} transients and sarcomere length shortening using an IonOptix CnC System (IonOptix) and analyzed using CytoSolver software (IonOptix).

Statistics

Statistical analysis was performed using unpaired, two-tailed Welch's T-test ($\alpha = 0.05$), ANOVA (one-way, two-way, or repeated measures) followed by Tukey HSD post-hoc tests ($\alpha = 0.05$), and Kaplan-Meier estimator analyses ($\alpha = 0.05$), where appropriate. A P-value less than 0.05 was considered significant. Data are displayed as mean ± SEM, box-and-whisker plots, or survival curves.

Study Approval

All animal studies were approved and conducted in accordance with the University of Florida IACUC.

Data Availability

The datasets generated during and/or analyzed during the current study are available in the Supporting data values file associated with this publication.

ACKNOWLEDGMENTS

This work was funded by a Wellstone Muscular Dystrophy Cooperative Center grant (P50-AR-052646) from the NIH to HLS and DWH, a Parent Project Muscular Dystrophy grant to HLS. GG is supported by grants from NIH (R01NS076991-01, 1P01AI100263-01, 4P01HL131471-02, UG3 HL147367-01, and R01HL097088). Michael Matheny, Heejae Chun, Jeffrey Herr, Spencer Henley-Beasley, Kara Pugliese, and Lillian Wright are thanked for their technical support related to this project.

AUTHOR CONTRIBUTIONS

Study design was contributed by CCH, YL, DWH, and HLS. Experimental procedures and data acquisition were conducted by CCH, YL, BLL and DWH. Essential reagents were produced and provided by JX and GG. All authors were involved in data analysis, interpretation, data presentation, and manuscript writing.

Conflict of Interested Statement: The authors have declared no conflict of interest exists.

REFERENCES

1. Mendell JR, Shilling C, Leslie ND, Flanigan KM, al-Dahhak R, Gastier-Foster J, et al. Evidence-based path to newborn screening for Duchenne muscular dystrophy. *Ann Neurol.* 2012;71(3):304-13.

2. Hoffman EP, Brown RH, Jr., and Kunkel LM. Dystrophin: the protein product of the Duchenne muscular dystrophy locus. *Cell.* 1987;51(6):919-28.

3. Petrof BJ, Shrager JB, Stedman HH, Kelly AM, and Sweeney HL. Dystrophin protects the sarcolemma from stresses developed during muscle contraction. *Proc Natl Acad Sci U S A.* 1993;90(8):3710-4.

4. Wahlgren L, Kroksmark AK, Tulinius M, and Sofou K. One in five patients with Duchenne muscular dystrophy dies from other causes than cardiac or respiratory failure. *Eur J Epidemiol.* 2022;37(2):147-56.

5. Su JA, Ramos-Platt L, and Menteer J. Left Ventricular Tonic Contraction as a Novel Biomarker of Cardiomyopathy in Duchenne Muscular Dystrophy. *Pediatr Cardiol.* 2016;37(4):678-85.

6. Amedro P, Vincenti M, De La Villeon G, Lavastre K, Barrea C, Guillaumont S, et al. Speckle-Tracking Echocardiography in Children With Duchenne Muscular Dystrophy: A Prospective Multicenter Controlled Cross-Sectional Study. *J Am Soc Echocardiogr.* 2019;32(3):412-22.

7. Panovsky R, Pesl M, Machal J, Holecek T, Feitova V, Jurikova L, et al. Quantitative assessment of left ventricular longitudinal function and myocardial deformation in Duchenne muscular dystrophy patients. *Orphanet J Rare Dis.* 2021;16(1):57.

8. Batra A, Barnard AM, Lott DJ, Willcocks RJ, Forbes SC, Chakraborty S, et al. Longitudinal changes in cardiac function in Duchenne muscular dystrophy population as measured by magnetic resonance imaging. *BMC Cardiovasc Disord.* 2022;22(1):260.

9. Wang B, Li J, and Xiao X. Adeno-associated virus vector carrying human minidystrophin genes effectively ameliorates muscular dystrophy in mdx mouse model. *Proc Natl Acad Sci U S A.* 2000;97(25):13714-9.

10. Harper SQ, Hauser MA, DelloRusso C, Duan D, Crawford RW, Phelps SF, et al. Modular flexibility of dystrophin: implications for gene therapy of Duchenne muscular dystrophy. *Nat Med.* 2002;8(3):253-61.

11. Goyenvalle A, Vulin A, Fougerousse F, Leturcq F, Kaplan JC, Garcia L, et al. Rescue of dystrophic muscle through U7 snRNA-mediated exon skipping. *Science.* 2004;306(5702):1796-9.

12. Bish LT, Sleeper MM, Forbes SC, Wang B, Reynolds C, Singletary GE, et al. Long-term restoration of cardiac dystrophin expression in golden retriever muscular dystrophy following rAAV6-mediated exon skipping. *Mol Ther.* 2012;20(3):580-9.

13. Hammers DW, Hart CC, Matheny MK, Wright LA, Armellini M, Barton ER, et al. The D2.mdx mouse as a preclinical model of the skeletal muscle pathology associated with Duchenne muscular dystrophy. *Sci Rep.* 2020;10(1):14070.

14. Guo LJ, Soslow JH, Bettis AK, Nghiem PP, Cummings KJ, Lenox MW, et al. Natural History of Cardiomyopathy in Adult Dogs With Golden Retriever Muscular Dystrophy. *J Am Heart Assoc.* 2019;8(16):e012443.

15. Schneider SM, Sansom GT, Guo LJ, Furuya S, Weeks BR, and Kornegay JN. Natural History of Histopathologic Changes in Cardiomyopathy of Golden Retriever Muscular Dystrophy. *Front Vet Sci.* 2021;8:759585.

16. Markati T, De Waele L, Schara-Schmidt U, and Servais L. Lessons Learned from Discontinued Clinical Developments in Duchenne Muscular Dystrophy. *Front Pharmacol.* 2021;12:735912.

17. Fukada S, Morikawa D, Yamamoto Y, Yoshida T, Sumie N, Yamaguchi M, et al. Genetic background affects properties of satellite cells and mdx phenotypes. *Am J Pathol.* 2010;176(5):2414-24.

18. Coley WD, Bogdanik L, Vila MC, Yu Q, Van Der Meulen JH, Rayavarapu S, et al. Effect of genetic background on the dystrophic phenotype in mdx mice. *Hum Mol Genet.* 2016;25(1):130-45.

19. Chu X, Li J, Qiao C, Wang J, Wang Y, Jiang XC, et al. Long-term effect of human mini-dystrophin in transgenic mdx mice improves muscle physiological function. *FASEB J.* 2021;35(6):e21628.

20. Himeda CL, Chen X, and Hauschka SD. Design and testing of regulatory cassettes for optimal activity in skeletal and cardiac muscles. *Methods Mol Biol.* 2011;709:3-19.

21. Ai J, Li J, Gessler DJ, Su Q, Wei Q, Li H, et al. Adeno-associated virus serotype rh.10 displays strong muscle tropism following intraperitoneal delivery. *Sci Rep.* 2017;7:40336.

22. Duan D. Systemic AAV Micro-dystrophin Gene Therapy for Duchenne Muscular Dystrophy. *Mol Ther.* 2018;26(10):2337-56.

688 23. Mendell JR, Sahenk Z, Lehman K, Nease C, Lowes LP, Miller NF, et al. Assessment of
689 Systemic Delivery of rAAVrh74.MHCK7.micro-dystrophin in Children With Duchenne
690 Muscular Dystrophy: A Nonrandomized Controlled Trial. *JAMA Neurol.* 2020.

691 24. Hakim CH, Wasala NB, Pan X, Kodippili K, Yue Y, Zhang K, et al. A Five-Repeat Micro-
692 Dystrophin Gene Ameliorated Dystrophic Phenotype in the Severe DBA/2J-mdx Model of
693 Duchenne Muscular Dystrophy. *Mol Ther Methods Clin Dev.* 2017;6:216-30.

694 25. Ramos JN, Hollinger K, Bengtsson NE, Allen JM, Hauschka SD, and Chamberlain JS.
695 Development of Novel Micro-dystrophins with Enhanced Functionality. *Mol Ther.*
696 2019;27(3):623-35.

697 26. Matsumura K, Ervasti JM, Ohlendieck K, Kahl SD, and Campbell KP. Association of
698 dystrophin-related protein with dystrophin-associated proteins in mdx mouse muscle.
699 *Nature.* 1992;360(6404):588-91.

700 27. Weir AP, Burton EA, Harrod G, and Davies KE. A- and B-utrophin have different
701 expression patterns and are differentially up-regulated in mdx muscle. *J Biol Chem.*
702 2002;277(47):45285-90.

703 28. Hammers DW, Sleeper MM, Forbes SC, Shima A, Walter GA, and Sweeney HL. Tadalafil
704 Treatment Delays the Onset of Cardiomyopathy in Dystrophin-Deficient Hearts. *J Am*
705 *Heart Assoc.* 2016;5(8).

706 29. Grady RM, Teng H, Nichol MC, Cunningham JC, Wilkinson RS, and Sanes JR. Skeletal
707 and cardiac myopathies in mice lacking utrophin and dystrophin: a model for Duchenne
708 muscular dystrophy. *Cell.* 1997;90(4):729-38.

30. Janssen PM, Hiranandani N, Mays TA, and Rafael-Fortney JA. Utrophin deficiency worsens cardiac contractile dysfunction present in dystrophin-deficient mdx mice. *Am J Physiol Heart Circ Physiol.* 2005;289(6):H2373-8.

31. Rafael-Fortney JA, Chimanji NS, Schill KE, Martin CD, Murray JD, Ganguly R, et al. Early treatment with lisinopril and spironolactone preserves cardiac and skeletal muscle in Duchenne muscular dystrophy mice. *Circulation.* 2011;124(5):582-8.

32. Bewick GS, Nicholson LV, Young C, O'Donnell E, and Slater CR. Different distributions of dystrophin and related proteins at nerve-muscle junctions. *Neuroreport.* 1992;3(10):857-60.

33. Sealock R, Butler MH, Kramarcy NR, Gao KX, Murnane AA, Douville K, et al. Localization of dystrophin relative to acetylcholine receptor domains in electric tissue and adult and cultured skeletal muscle. *J Cell Biol.* 1991;113(5):1133-44.

34. Flucher BE, and Daniels MP. Distribution of Na+ channels and ankyrin in neuromuscular junctions is complementary to that of acetylcholine receptors and the 43 kd protein. *Neuron.* 1989;3(2):163-75.

35. Byers TJ, Kunkel LM, and Watkins SC. The subcellular distribution of dystrophin in mouse skeletal, cardiac, and smooth muscle. *J Cell Biol.* 1991;115(2):411-21.

36. Sealock R, Wray BE, and Froehner SC. Ultrastructural localization of the Mr 43,000 protein and the acetylcholine receptor in Torpedo postsynaptic membranes using monoclonal antibodies. *J Cell Biol.* 1984;98(6):2239-44.

37. Wood SJ, and Slater CR. beta-Spectrin is colocalized with both voltage-gated sodium channels and ankyrinG at the adult rat neuromuscular junction. *J Cell Biol.* 1998;140(3):675-84.

38. Salpeter MM, and Loring RH. Nicotinic acetylcholine receptors in vertebrate muscle: properties, distribution and neural control. *Prog Neurobiol.* 1985;25(4):297-325.

39. McLendon PM, and Robbins J. Proteotoxicity and cardiac dysfunction. *Circ Res.* 2015;116(11):1863-82.

40. Galvez AS, Diwan A, Odley AM, Hahn HS, Osinska H, Melendez JG, et al. Cardiomyocyte degeneration with calpain deficiency reveals a critical role in protein homeostasis. *Circ Res.* 2007;100(7):1071-8.

41. Predmore JM, Wang P, Davis F, Bartolone S, Westfall MV, Dyke DB, et al. Ubiquitin proteasome dysfunction in human hypertrophic and dilated cardiomyopathies. *Circulation.* 2010;121(8):997-1004.

42. Gilda JE, and Gomes AV. Proteasome dysfunction in cardiomyopathies. *J Physiol.* 2017;595(12):4051-71.

43. Hart C, Lee Yi, Hammers D, and Sweeney L. Evaluation of the DBA/2J mouse as a potential background strain for genetic models of cardiomyopathy. 2022;1.

44. Odom GL, Gregorevic P, Allen JM, and Chamberlain JS. Gene therapy of mdx mice with large truncated dystrophins generated by recombination using rAAV6. *Mol Ther.* 2011;19(1):36-45.

45. Banks GB, Judge LM, Allen JM, and Chamberlain JS. The polyproline site in hinge 2 influences the functional capacity of truncated dystrophins. *PLoS Genet.* 2010;6(5):e1000958.

46. Potter RA, Griffin DA, Heller KN, Peterson EL, Clark EK, Mendell JR, et al. Dose-Escalation Study of Systemically Delivered rAAVrh74.MHCK7.micro-dystrophin in the mdx Mouse Model of Duchenne Muscular Dystrophy. *Hum Gene Ther.* 2021;32(7-8):375-89.

47. Townsend D, Blankinship MJ, Allen JM, Gregorevic P, Chamberlain JS, and Metzger JM. Systemic administration of micro-dystrophin restores cardiac geometry and prevents dobutamine-induced cardiac pump failure. *Mol Ther.* 2007;15(6):1086-92.

48. Bostick B, Shin JH, Yue Y, and Duan D. AAV-microdystrophin therapy improves cardiac performance in aged female mdx mice. *Mol Ther.* 2011;19(10):1826-32.

49. Schinkel S, Bauer R, Bekeredjian R, Stucka R, Rutschow D, Lochmuller H, et al. Long-term preservation of cardiac structure and function after adeno-associated virus serotype 9-mediated microdystrophin gene transfer in mdx mice. *Hum Gene Ther.* 2012;23(6):566-75.

50. Bostick B, Shin JH, Yue Y, Wasala NB, Lai Y, and Duan D. AAV micro-dystrophin gene therapy alleviates stress-induced cardiac death but not myocardial fibrosis in >21-m-old mdx mice, an end-stage model of Duchenne muscular dystrophy cardiomyopathy. *J Mol Cell Cardiol.* 2012;53(2):217-22.

51. Bönnemann CG, Belluscio BA, Braun S, Morris C, Singh T, and Muntoni F. Dystrophin Immunity after Gene Therapy for Duchenne's Muscular Dystrophy. *N Engl J Med.* 2023;388(24):2294-6.

52. Pacak CA, Mah CS, Thattaliyath BD, Conlon TJ, Lewis MA, Cloutier DE, et al. Recombinant adeno-associated virus serotype 9 leads to preferential cardiac transduction in vivo. *Circ Res.* 2006;99(4):e3-9.

53. Salva MZ, Himeda CL, Tai PW, Nishiuchi E, Gregorevic P, Allen JM, et al. Design of tissue-specific regulatory cassettes for high-level rAAV-mediated expression in skeletal and cardiac muscle. *Mol Ther.* 2007;15(2):320-9.

54. Walklate J, Ferrantini C, Johnson CA, Tesi C, Poggesi C, and Geeves MA. Alpha and beta myosin isoforms and human atrial and ventricular contraction. *Cell Mol Life Sci.* 2021;78(23):7309-37.

55. England SB, Nicholson LV, Johnson MA, Forrest SM, Love DR, Zubrzycka-Gaarn EE, et al. Very mild muscular dystrophy associated with the deletion of 46% of dystrophin. *Nature.* 1990;343(6254):180-2.

56. Passos-Bueno MR, Vainzof M, Marie SK, and Zatz M. Half the dystrophin gene is apparently enough for a mild clinical course: confirmation of its potential use for gene therapy. *Hum Mol Genet.* 1994;3(6):919-22.

57. Johnson EK, Zhang L, Adams ME, Phillips A, Freitas MA, Froehner SC, et al. Proteomic analysis reveals new cardiac-specific dystrophin-associated proteins. *PLoS One.* 2012;7(8):e43515.

58. Kaspar RW, Allen HD, Ray WC, Alvarez CE, Kissel JT, Pestronk A, et al. Analysis of dystrophin deletion mutations predicts age of cardiomyopathy onset in becker muscular dystrophy. *Circ Cardiovasc Genet.* 2009;2(6):544-51.

59. Cooper-Olson G, Rodino-Klapac LR, and Potter RA. Evaluation of the Lipid-binding Properties of Recombinant Dystrophin Spectrin-like Repeat Domains R1-3. *J Neuromuscul Dis.* 2021;8(4):489-94.

60. Howard ZM, Dorn LE, Lowe J, Gertzen MD, Ciccone P, Rastogi N, et al. Micro-dystrophin gene therapy prevents heart failure in an improved Duchenne muscular dystrophy cardiomyopathy mouse model. *JCI Insight.* 2021;6(7).

61. Krishna S, Piepho AB, Lake DM, Cumby LR, Lortz KK, Lowe J, et al. Gene therapy delivered micro-dystrophins co-localize with transgenic utrophin in dystrophic skeletal muscle fibers. *Neuromuscul Disord.* 2024;36:1-5.

62. Cui W, Jang A, Zhang P, Thompson B, Townsend D, Metzger JM, et al. Early Detection of Myocardial Bioenergetic Deficits: A 9.4 Tesla Complete Non Invasive 31P MR Spectroscopy Study in Mice with Muscular Dystrophy. *PLoS One.* 2015;10(8):e0135000.

63. Yue Y, Wasala NB, Bostick B, and Duan D. 100-fold but not 50-fold dystrophin overexpression aggravates electrocardiographic defects in the mdx model of Duchenne muscular dystrophy. *Mol Ther Methods Clin Dev.* 2016;3:16045.

64. Levitt N, Briggs D, Gil A, and Proudfoot NJ. Definition of an efficient synthetic poly(A) site. *Genes Dev.* 1989;3(7):1019-25.

65. Sena-Esteves M, and Gao G. Introducing Genes into Mammalian Cells: Viral Vectors. *Cold Spring Harb Protoc.* 2020;2020(8):pdb top095513.

66. Hammers DW, Sleeper MM, Forbes SC, Coker CC, Jirousek MR, Zimmer M, et al. Disease-modifying effects of orally bioavailable NF-kappaB inhibitors in dystrophin-deficient muscle. *JCI Insight.* 2016;1(21):e90341.

67. Kim MJ, Whitehead NP, Bible KL, Adams ME, and Froehner SC. Mice lacking alpha-, beta1- and beta2-syntrophins exhibit diminished function and reduced dystrophin expression in both cardiac and skeletal muscle. *Hum Mol Genet.* 2019;28(3):386-95.

TABLES

MDC	Lifespan	Diaphragm specific force	EDL Max Force	EDL Specific Force	Protection against EDL eccentric damage	Skeletal muscle fibrosis	Cardiac Outcome
1	↓	↔	↑	↔	↑	↓	DCM
2	↔	↑	↑	↑	↑	↓	RCM (12mo) DCM (18mo)
3	↔	↔	↑	↑	↔	↓	↑
4	↓	↑	↑	↔	↑	↓	DCM

Table 1. Phenotype summary from micro-dystrophin pre-clinical study

FIGURES

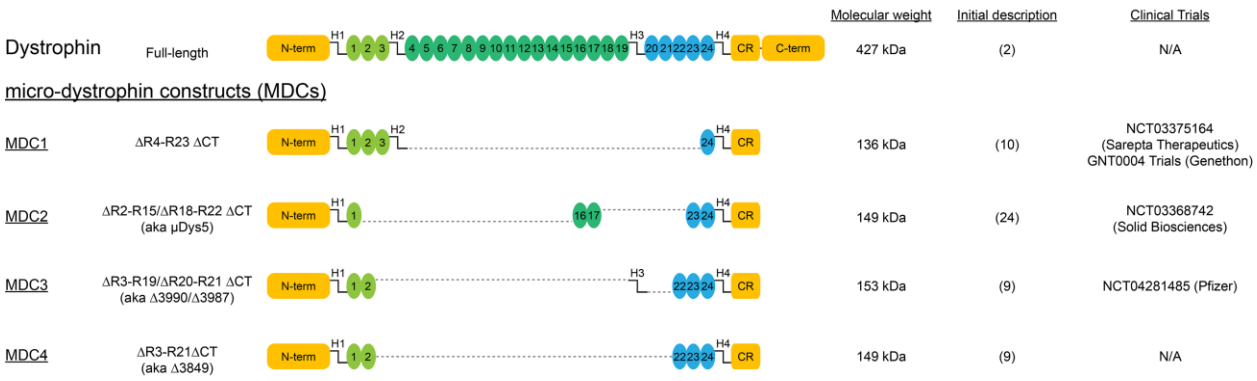

Figure 1. Structure of dystrophin and micro-dystrophin constructs. A schematic diagram of full-length dystrophin, the **m**icro-**d**ystrophin **c**onstructs (MDCs) currently utilized in clinical trials (MDC1-3) as well as of MDC4, a modification of MDC3.

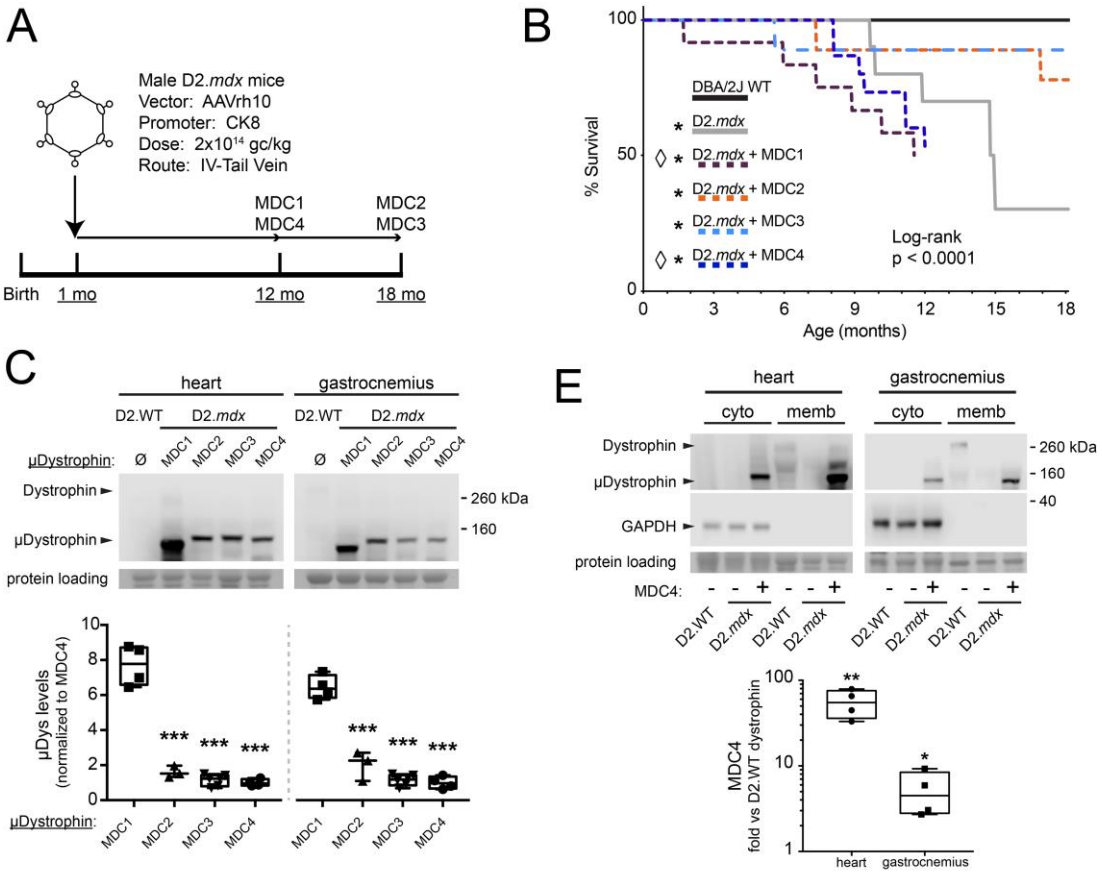
A
Male D2.mdx mice
Vector: AAVrh10
Promoter: CK8
Dose: 2x10^14 gc/kg
Route: IV-Tail Vein
MDC1
MDC4
MDC2
MDC3
Birth
1 mo
12 mo
18 mo
B
% Survival
Age (months)
DBA/2J WT
D2.mdx
D2.mdx + MDC1
D2.mdx + MDC2
D2.mdx + MDC3
D2.mdx + MDC4
Log-rank
p < 0.0001
C
heart
gastrocnemius
D2.WT
D2.mdx
µDystrophin:
Dystrophin
µDystrophin
protein loading
260 kDa
160
µDys levels
(normalized to MDC4)
E
heart
gastrocnemius
cyto
memb
Dystrophin
µDystrophin
GAPDH
protein loading
MDC4:
260 kDa
160
40
MDC4
fold vs D2.WT dystrophin
D
D2.WT
D2.mdx
µDys:
MDC1
MDC2
MDC3
MDC4
heart
gastrocnemius
Dystrophin (MANEX1011B)
β-DG
Syntrophin
Dystrobrevin

Figure 2. Adeno-associated virus-mediated striated muscle expression of micro-dystrophin constructs. (**A**) Male D2.*mdx* mice were injected with $2x10^{14}$ gc/kg of AAVrh10 carrying one for the 4 MCD4 transgenes placed behind the CK8, striated muscle, promoter via tail vein at one month of age. (**B**) Micro-dystrophin gene therapy can result in premature death. Survival curve of D2.WT, D2.*mdx* and D2.*mdx* mice treated with each of the 4 MDCs. None of the MDCs restored the lifespan of treated animals to that observed with DBA/2J WT animals (Pair-wise Log-rank test; * $p<0.05$ vs DBA/2J WT with Bonferroni correction). Two of the micro-dystrophin constructs tested (mDC1 and mDC4) led to premature death of treated mice (Pair-wise Log-rank test; ◊ $p<0.05$ vs D2.*mdx* with Bonferroni correction). (**C**) Western blots of lysates of heart and gastrocnemius muscles from D2.*mdx* animals each transduced with one of the four MDCs. The 5-repeat MDCs examined (MDC2-4) show similar expression in both muscles, while the 4-repeat MDC1 was expressed at levels several-fold higher in comparison (~8- and ~6-fold higher in heart and gastrocnemius, respectively; n=3-6, $p<000.1$, One-way ANOVA; *** $p<0.001$ vs mDC1, Tukey post-hoc comparison). (**D**) Comparison of mDC4 expression vs endogenous full-length dystrophin in heart and gastrocnemius showed ~50- and ~5-fold overexpression, respectively (n=4, Student's t-test, * $p<0.05$, ** $p<0.01$). In addition, in agreement with the antibody-mediated labeling of MDC4 (c), a large majority of MDC4 was found to be associated with the membrane-enriched fraction of each tissue. (**E**) Top four rows: Antibody-mediated labeling of heart transverse sections from D2.WT, D2.*mdx* and D2.*mdx* mice treated with each of the 4 MDCs revealed sarcolemmal localization of micro-dystrophin proteins that mirror sarcolemmal localization of full-length endogenous dystrophin protein in D2.WT cardiomyocytes. Concurrently, over-expression of each MDC also restores sarcolemmal localization of the DGC components β-dystroglycan (β-DG), syntrophin, and dystrobrevin. Bottom row: Antibody-mediated labeling of gastrocnemius transverse sections from D2.WT, D2.*mdx* and D2.*mdx* mice treated with each of the 4 MDCs examined at terminal time points (12m for MDCs 1 & 4; 18m for MDCs 2 &3) demonstrated maintained sarcolemmal localization of each of the 4 MDCs that mirror sarcolemmal localization of full-length endogenous dystrophin protein until the study endpoints. Box-and-Whisker plots: minimum-to-maximum with 2nd and 3rd quartiles within the box with a line that indicates the mean. Scale bars: 100 μm.

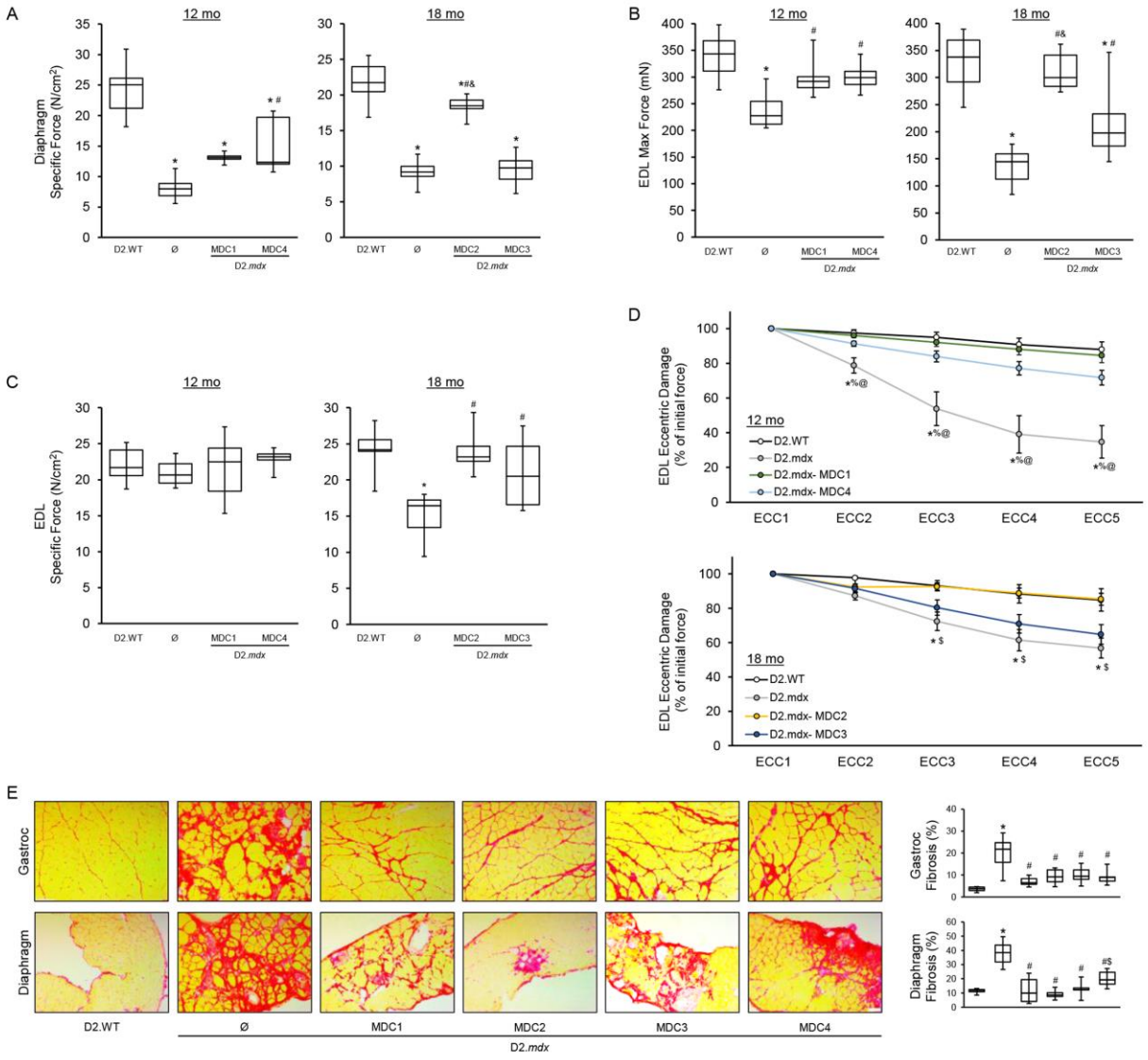

Figure 3. Micro-dystrophin provides partial rescue of D2.*mdx* skeletal muscle. Male D2.*mdx* mice were treated with micro-dystrophin (µDys) gene therapy at 1 month of age (mo; refer to **Figure 2a**). At the terminal endpoints of 12- and 18- mo, *ex vivo* muscle function was performed for the (**a**) diaphragm and (**b-d**) extensor digitorum longus muscles (EDL) of D2.WT, untreated D2.*mdx*, and µDys-treated D2.*mdx* mice (n = 6-10). Representative picrosirius red-stained images of the gastrocnemius and diaphragm muscles with accompanying fibrosis quantifications for these groups (**e**). Scale bar = 75µm. Data were analyzed using one-way ANOVA with Tukey HSD post-hoc tests (α = 0.05) and displayed as (**A-C**, **E**) box-and-whisker plots (boxes indicate 2nd and 3rd quartiles and error bars represent the minimum and maximum values) or mean ± SEM. *p<0.05 compared to WT; #p<0.05 compared to untreated D2.*mdx*; %p<0.05 compared to MDC1; $p<0.05 compared to MDC2; &p<0.05 compared to MDC3; @p<0.05 compared to MDC4.

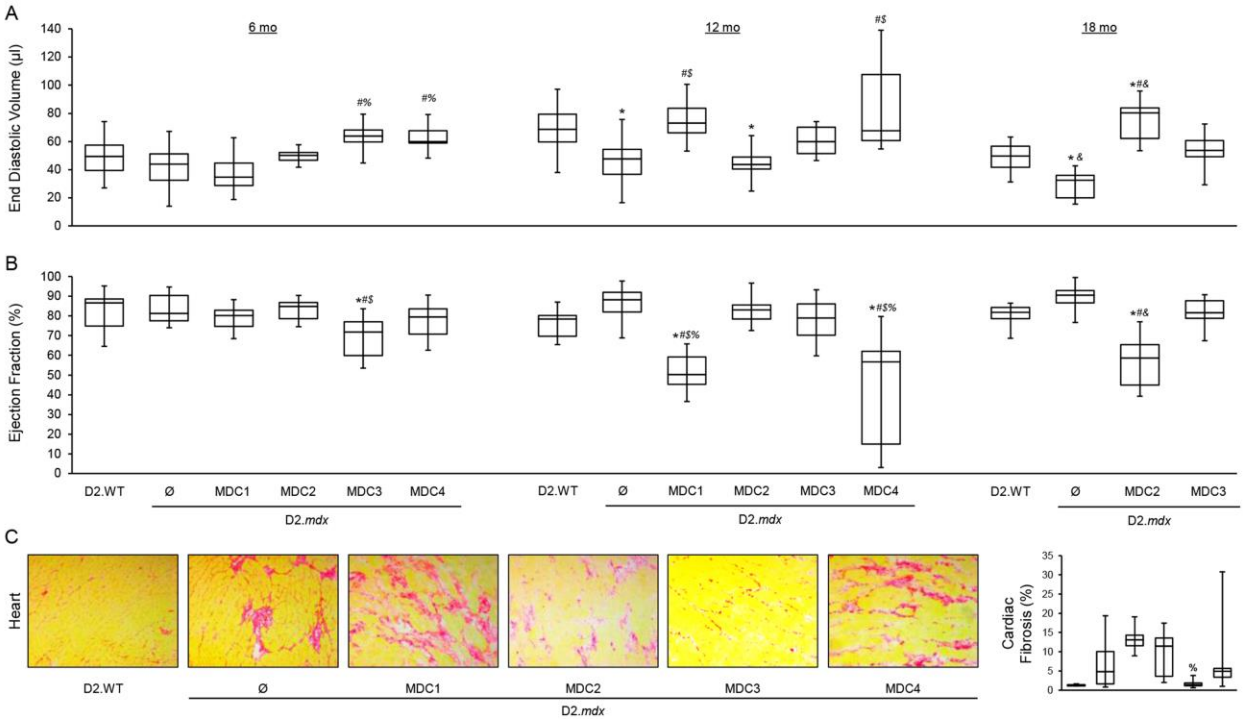

Figure 4. Long-term micro-dystrophin expression causes cardiomyopathy in D2.*mdx* mice. Male D2.*mdx* mice were treated with micro-dystrophin (µDys) gene therapy at 1 month of age (mo; refer to **Figure 2a**). End diastolic volume (**a**) and ejection fraction (**b**) were measured in D2.WT, untreated D2.*mdx*, and µDys-treated D2.*mdx* mice at 6, 12 and 18 months of age. Representative picrosirius red-stained images of the heart with accompanying fibrosis quantifications for these groups (**c**). Scale bar = 75µm. Data were analyzed using one-way ANOVA with Tukey HSD post-hoc tests ($\alpha = 0.05$) and displayed as (**A-C**, **E**) box-and-whisker plots (boxes indicate 2nd and 3rd quartiles and error bars represent the minimum and maximum values). *p < 0.05 vs. D2.WT values; #p < 0.05 vs. D2.*mdx* values; %p<0.05 vs. MDC1 values; $p<0.05 vs. MDC2 values; &p<0.05 vs. MDC3 values.

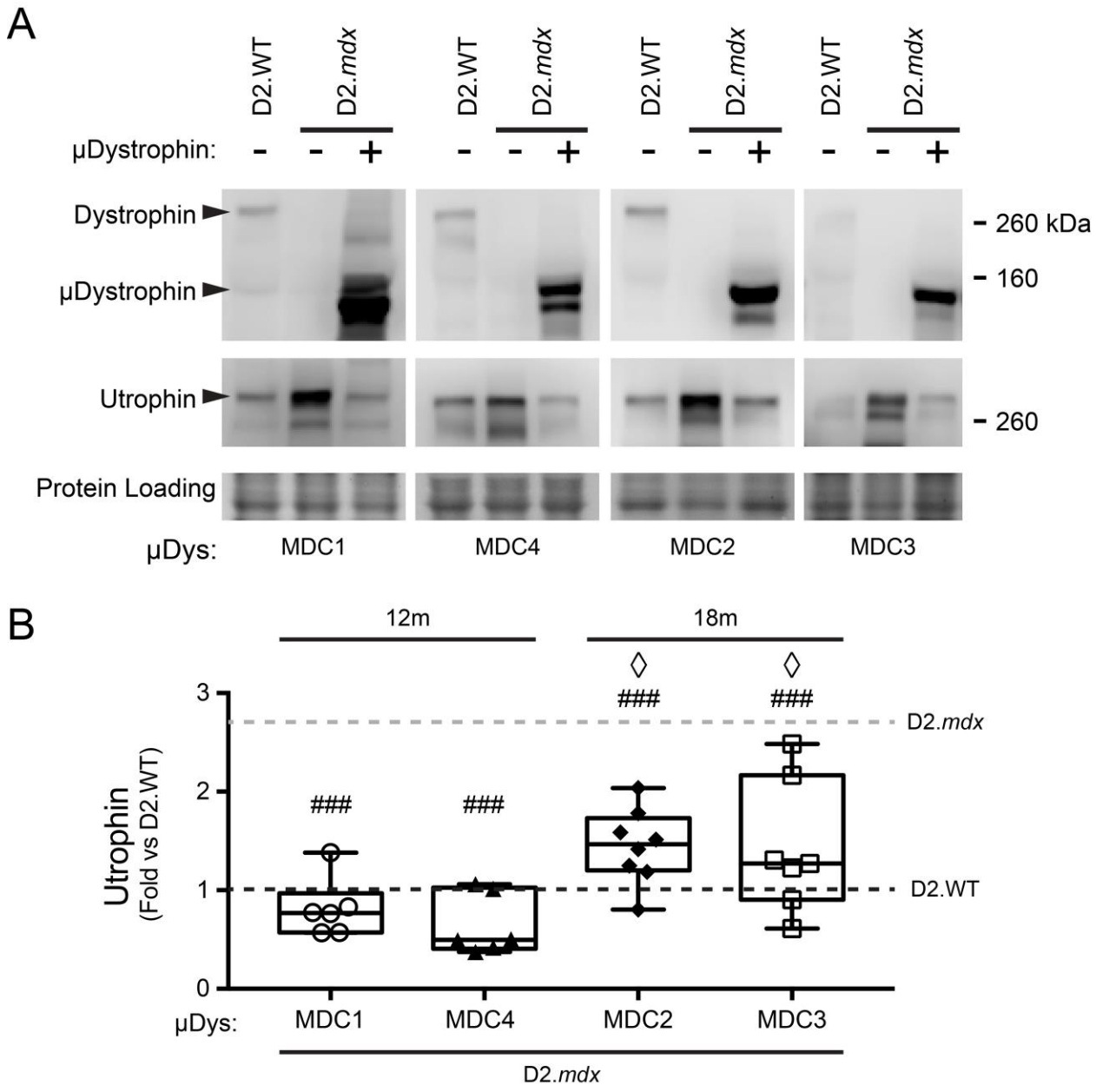

Figure 5. Diminution of sarcolemmal utrophin in micro-dystrophin overexpressing hearts. Western blots of plasma membrane-enriched heart samples reveal an approximately 2-3-fold upregulation of membrane-associated utrophin in D2.*mdx* (n=16, grey dotted line). This increased membrane-associated utrophin was normalized to D2.WT levels (black dotted line) in the heart upon AAV-mediated overexpression of MDC2 (n=8) or MDC4 (n=7) and even reduced to approximately 60% of the D2.WTs upon over-expression of MDC1 (n=6) or MDC4 (n=6) (One-way ANOVA; *** p<0.001 vs D2.WT, ### p<0.001 vs D2.*mdx*, ◊ p<0.05 vs D2.*mdx* + MDC4, Tukey post-hoc comparison). Box-and-Whisker plots: minimum-to-maximum with 2nd and 3rd quartiles within the box with a line that indicates the mean.